Computational Analysis of a Zn-Bound Tris(imidazolyl) Calix[6]arene Aqua Complex: Toward Incorporating Second-Coordination Sphere Effects into Carbonic Anhydrase Biomimetics

Lucas Koziol,[‡] Sebnem G. Essiz,[†,‡] Sergio E. Wong,[‡] Edmond Y. Lau,[‡] Carlos A. Valdez,[‡] Joe H. Satcher, Jr.,[‡] Roger D. Aines,*[‡] and Felice C. Lightstone*[‡]

[†]Bioinformatics and Genetics Department, Faculty of Engineering and Natural Sciences, Kadir Has University, 34083 Fatih, Istanbul, Turkey

[‡]Lawrence Livermore National Laboratory, 7000 East Avenue, Livermore, California 94550, United States

S *Supporting Information*

ABSTRACT: Molecular dynamics simulations and quantum-mechanical calculations were performed to characterize a supramolecular tris(imidazolyl) calix[6]arene Zn^{2+} aqua complex, as a biomimetic model for the catalyzed hydration of carbon dioxide to bicarbonate, $H_2O + CO_2 \rightarrow H^+ + HCO_3^-$. On the basis of potential-of-mean-force (PMF) calculations, stable conformations had distorted 3-fold symmetry and supported either one or zero encapsulated water molecules. The conformation with an encapsulated water molecule is calculated to be lower in free energy than the conformation with an empty cavity ($\Delta G = 1.2$ kcal/mol) and is the calculated free-energy minimum in solution. CO_2 molecule partitioning into the cavity is shown to be very facile, proceeding with a barrier of 1.6 kcal/mol from a weak encounter complex which stabilizes the species by about 1.0 kcal/mol. The stabilization energy of CO_2 is calculated to be larger than that of H_2O ($\Delta\Delta G = 1.4$ kcal/mol), suggesting that the complex will preferentially encapsulate CO_2 in solution. In contrast, the PMF for a bicarbonate anion entering the cavity is calculated to be repulsive in all nonbonding regions of the cavity, due to the diameter of the calix[6]arene walls. Geometry optimization of the Zn-bound hydroxide complex with an encapsulated CO_2 molecule showed that multiple noncovalent interactions direct the reactants into optimal position for nucleophilic addition to occur. The calixarene complex is a structural mimic of the hydrophilic/hydrophobic divide in the enzyme, providing a functional effect for CO_2 addition in the catalytic cycle. The results show that Zn-binding calix[6]arene scaffolds can be potential synthetic biomimetics for CO_2 hydration catalysis, both in terms of preferentially encapsulating CO_2 from solution and by spatially fixing the reactive species inside the cavity.
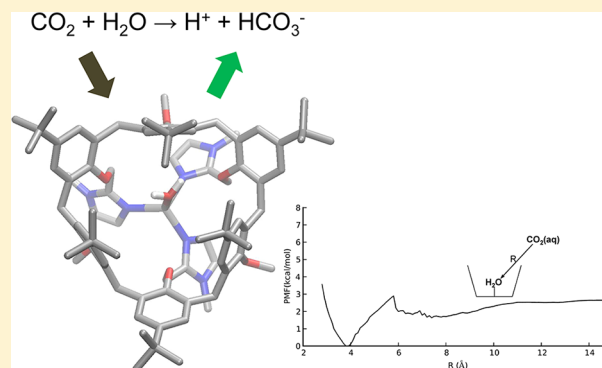
1. INTRODUCTION

Carbonic anhydrase (CA) is one of the fastest enzymes in nature, catalyzing the reversible hydration of carbon dioxide with a rate constant on the order of 10^6 M^{-1} s^{-1}.[1−3] In most mammalian CAs, the active site contains a tetrahedral Zn atom coordinated to three histidine sp^2 nitrogens and one water molecule oxygen. This Zn-bound water molecule is referred to as the aqua ligand throughout this article. A main effect of the tris(histidine) first-coordination sphere is to modulate the Lewis acidity of Zn, lowering the pK_a of the water from 15.7 to around 7.[4] The enzyme can thus provide a nucleophilic hydroxide at biological pH. The steps in the Zn-bound hydroxide mechanism of the catalytic cycle are shown in Figure 1. In step 1, the hydroxide reacts with a molecule of CO_2 via nucleophilic addition, to form Zn-bound bicarbonate. In step 2, this bicarbonate is displaced from the Zn (requiring breaking of one or two Zn−O bonds, depending on monodentate or bidentate binding) by a second water molecule. The mechanism of this substitution reaction (particularly, whether it proceeds via associative or dissociative mechanism) has not yet been conclusively established. A volume profile analysis concluded that substitution occurs via a dissociative mechanism,[3] although this has not been considered conclusive.[2,5] In step 3, the Zn-bound water is deprotonated, and the excess proton must be transported from the active site to bulk solvent. In the enzyme, shuttling this proton from the aqua ligand to the solvent is the rate-limiting step,[6,7] proceeding via a water network spanning 8−10 Å and, in some CAs, also utilizing a basic histidine which undergoes an intramolecular proton transfer.[8,9]

In addition to the three Zn-coordinating histidines, the protein "second-coordination sphere" (defined as nearby residues which interact with Zn-bound aqua and bicarbonate
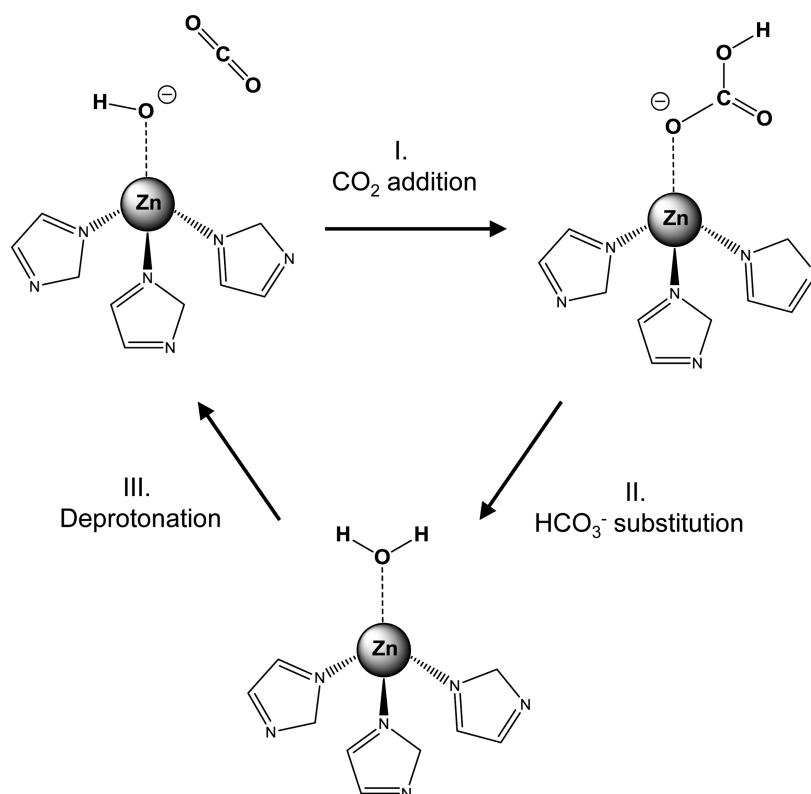
Figure 1. The Zn-bound hydroxide mechanism of the CO_2 hydration catalytic cycle, showing the Zn^{2+} first-coordination shell.

through noncovalent interactions) also plays a critical role in determining the extremely fast turnover rate.[10,11] The active site is funnel-shaped, with hydrophobic and hydrophilic residues occupying opposite sides of the cavity. Hydrophobic residues localize CO_2 in position adjacent to the Zn-bound hydroxide lone pairs, thereby facilitating step 1 in the catalytic cycle. Hydrophilic residues also play important functions. These include polarization of CO_2 through hydrogen-bonding interactions (step 1), destabilization of Zn-bound bicarbonate (step 2), and lowering the pK_a of the Zn-bound water (step 3). Two encapsulated waters inside the active site are thought to be important for displacing bicarbonate from Zn,[12] as well as for shuttling the excess proton out to the bulk solvent (e.g., by a Grotthus-like mechanism).[7,13]

A large amount of previous work has focused on developing simplified, model systems of the CA active site to recover some part of the enzyme's activity in more tractable systems.[14–22] Anders and co-workers identified the equilibrium geometries and saddle points for the model complex $(NH_3)_3Zn^{2+}(OH^-)$ + CO_2 using DFT (B3LYP/6-311+G(d,p)).[14] A number of experimental studies have applied the biomimetic approach using inorganic, metal-binding ligands toward CO_2 binding or conversion.[15–22] Detailed kinetic studies of two prototypical aza-macrocyclic ligands were reported by van Eldik and co-workers.[15,16] These studies established that only the deprotonated (hydroxide) form of the aqua ligand is catalytic, supporting a "nucleophilic hydroxide" mechanism. Experimental studies on a series of tris(pyrazolyl)hydroborate Cd^{2+} ligands suggested that the unidentate bicarbonate binding mode is necessary for efficient catalysis, because the degree of unidentate character upon metal substitution correlated with activity in the corresponding metal-substituted CA.[23] An analysis of catalytic activity and the mechanism for a series of

aza-macrocyclic ligands was recently reported by us.[24] This joint theoretical–experimental study found that for first-coordination sphere catalysts, optimizing the rate constant is a balance between minimizing the Lewis acidity of the ligand–Zn^{2+} complex and maintaining the pK_a low enough to deprotonate the aqua ligand under the experimental conditions. To date, no experimental or computational study (to our knowledge) has examined the effects of a second-coordination sphere on the essential reactive center shown in Figure 1, despite its known importance in CA. For example, Thr199 is a hydrogen-bond acceptor in the HCA second-coordination sphere, and single-point mutations to this residue or its H-bond partners result in 100× and 1000× reductions in activity, respectively, compared to the native enzyme.[10] The most active synthetic CA mimic in water is currently cyclen, which lacks a second-coordination sphere entirely and has a measured k_{cat} of about 3000 M^{-1} s^{-1} at pH 9.[16,24] Cyclen, and especially next-generation improved biomimetics, have the potential to play significant roles in several technologies, particularly in industrial CO_2 capture.[25]

These previous studies motivate the present work. In this article, we characterize thermodynamic and kinetic properties of a calix[6]arene synthetic "proto-protein" pocket on the tris(imidazolyl) Zn^{2+} reactive center, in an aqueous environment using explicit solvent. We compare the structure of the H-bond network inside the cavity (by DFT and MD) with the crystal structure of a closely related complex (R = Et in Figure 6) reported by Reinaud and co-workers,[26] showing excellent agreement. Free-energy differences are obtained for single-molecule CO_2 and HCO_3^- partitioning between the cavity and bulk solvent. Finally, DFT optimization of the Zn-bound hydroxide complex with encapsulated CO_2 shows that the

calixarene pocket plays a significant role in preorganizing the reactants inside the cavity.

2. COMPUTATIONAL DETAILS

The Amber 10 program was used for all classical MD simulations.[27] Initial geometries were built using Maestro.[28] In MD simulations, the Generalized Amber Force Field (GAFF) was used for terms not including Zn.[29] Terms including Zn (bond and angle stretches; Zn dihedral terms were not included) were taken from a recent publication by Lin and Wang.[30] In all MD calculations, an explicitly bonded model was used for the Zn−O bond (connecting Zn^{2+} with the oxygen of the aqua ligand). Lin and Wang used several Zn^{2+} coordination environments common in biological settings to parametrize the model,[30] including bonds to three histidine nitrogens and one water oxygen (analogous to the complex considered here).

For treatment of electrostatics in MD, atomic partial charges were calculated from the HF/6-31G(d) density using the electrostatic potential (ESP) module in NWChem 6.0.[31] No restraints were used in the charge-fitting procedure; this may yield slightly more polarized charges compared to restrained ESP (RESP) fitting implemented in other software packages (e.g., Antechamber). Equilibrium, NVT dynamics was performed using a 1 fs time step, and with a particle mesh Ewald (PME) cutoff of 12.0 Å. The SHAKE algorithm was not used, because hydrogen motions could play a significant role in the dynamics. A rectangular TIP3P water box was used with minimum spacing of 15 Å in each direction. Temperature regulation was controlled by a Langevin dynamics scheme (ntt = 3) with collision frequency γ = 2.0, utilizing different random-number seeds for each calculation. The reciprocal sums in the force field were evaluated every four MD steps. Prior to each production run, at least 50 ps of equilibration was performed in the NPT ensemble with a pressure of 1 atm.

Umbrella sampling was performed with a single interatomic distance restraint, R, using a harmonic restraining potential

$$V^r(R; R_0) = \frac{1}{2}K(R - R_0)^2 \tag{1}$$

In all simulations, the window size ΔR was 0.1 Å, and the force constant K was fixed at 70.0 kcal/mol. This was found to give significant overlap in the histograms between adjacent windows. The umbrella-sampling path was defined by first creating a starting geometry at one window (typically, at small R with the substituent already enclosed) and then running short trajectories (25 ps) serially, changing the value of R by 0.1 Å to ensure a continuous path. Once this path was defined, production runs were run independently at each umbrella-sampling window. Sampling was run for time scales of at least 16.5 ns for all PMFs except Figure 11, which was long enough to converge all barriers to 0.1 kcal/mol. Statistics for the PMF calculation were taken from the last 5.5 ns. For the PMF for bicarbonate partitioning (Figure 11), sampling was performed for a total of 5.5 ns only. This is because high forces induced by restraining the bicarbonate inside an enclosed space eventually led to unphysical, irreversible "jumps," particularly inversion of the aqua ligand to point outside the cavity. The PMF obtained from the full 16.5 ns sampling time is shown in the Supporting Information and has very similar overall shape to that in Figure 11.

The PMFs were obtained from a restraint-based umbrella sampling pathway.[32] The mean force was calculated at each umbrella-sampling window, and the PMF was integrated numerically according to

$$F(R) = -\int_{R_0}^{R} \langle dV^r(R'; R_0) \rangle_{r, R'}\, dR' + 2kT \ln\left(\frac{R}{R_0}\right) + F(R_0) \tag{2}$$

R_0 is the value of R at an arbitrarily defined zero of free-energy. The second term arises from a Jacobian due to the non-Cartesian coordinate choice for V^r. The ensemble average in the first term equals $\langle K(R(r) - R_0) \rangle_{r, R'}$; this quantity was obtained from the MD trajectories. Similar integration methods have been used to evaluate free-energy curves for ion pairs in water[33] and barriers for molecular motions of rotaxane supramolecular complexes.[34]

All PMFs were also evaluated using the Weighted Histogram Analysis Method (WHAM), as provided by Grossfield and used unmodified.[35] A value of 100 for the bin number and convergence criterion of 0.0001 kcal/mol was used. The WHAM code does not take into account the non-Cartesian nature of R; therefore, it is also subject to the second term in eq 2, which was added analytically. Equation 2 and WHAM yielded essentially identical PMFs; both PMFs are provided in the Supporting Information (SI).

All MD calculations were performed with the protonated aqua ligand (Zn−H_2O). This allowed analysis of the full hydrogen-bond network and comparison with previously reported experimental data for this complex.[26] Steps 2 and 3 in the catalytic cycle include the protonated aqua ligand, while step 1 (CO_2 addition) only occurs with the deprotonated (Zn−OH^-) form. DFT calculations on the deprotonated complex with CO_2 are reported in section 3.4. CA mimics operate maximally at high pH (pH $\gg$ pK_a of aqua ligand) because of step 1 in the catalytic cycle.

Quantum-mechanical geometry optimizations and single-point energy calculations were carried out with the M06-2X meta-GGA density functional[36] and the 6-31G(d) basis set. While a larger basis set is required to obtain converged geometries, the large size of this system (about 210 atoms) precluded the use of larger basis sets in geometry optimizations. The M06 set of functionals has been parametrized to model short- and medium-range noncovalent interactions.[36] The choice of M06-2X was motivated by a previous benchmark study of DFT exchange-correlation functionals for various small ligand- Zn^{2+} complexes.[37] It was found that M06-2X was highly competitive in reproducing equilibrium geometries as well as bond-dissociation energies, as rated against CCSD results. NWChem, versions 6.0 and 6.1 were used for all DFT calculations.[31]

3. RESULTS AND DISCUSSION

The calixarene ring forms a cavity of approximately 50 Å³ surrounding the highly polar tris(imidazolyl) Zn−H_2O core. In solution, this cavity can be empty or filled by one or more water molecules, depending on the strength of noncovalent interactions between the substituents and the cavity. The previously reported crystal structure found a single buried water inside the cavity; however, the relative free-energies of empty and bound cavities have not been calculated. We first provide an analysis of the two conformations found for the empty cavity, followed by analysis of the calculated global free-energy minimum and its comparison with experiments.

3.1. States Containing an Empty Cavity. In all MD simulations of the empty cavity, only two different conformations could be observed. On the basis of running multiple trajectories from different starting configurations, every simulation showed the complex relaxing to one of these two conformations. Interconversion between these simulations was not observed in unrestrained simulations within the time scale of our simulations. Simulations using different partial charges (e.g., ESP fits at either of the two geometries) also did not reveal any other conformations. Both conformations were found to be minima on the (gas-phase) potential energy surface, at the M06-2X/6-31G(d) level. The two conformations are labeled CX_{3fs} and CX_{2fs}, shown in Figures 3 and 4, respectively. The label 3fs or 2fs corresponds to approximate 3-fold or 2-fold symmetry, respectively.
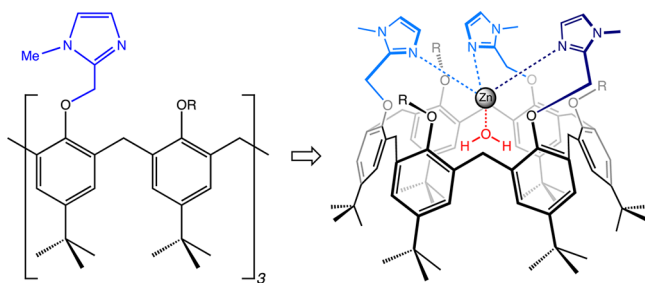

Figure 2. The tris(imidazolyl) calix[6]arene $Zn^{2+}-H_2O$ complex. R = Me (this work), Et (ref 38).
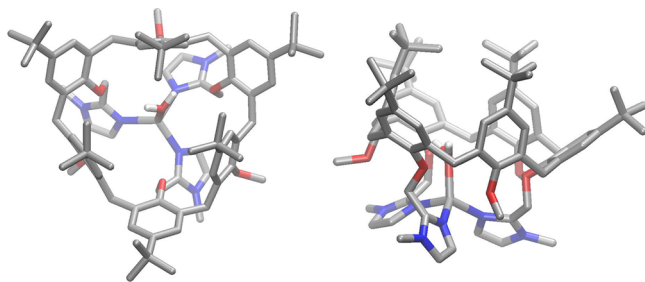

Figure 3. Top view (left) and side view (right) of CX_{3fs}. Most hydrogens are omitted for clarity.
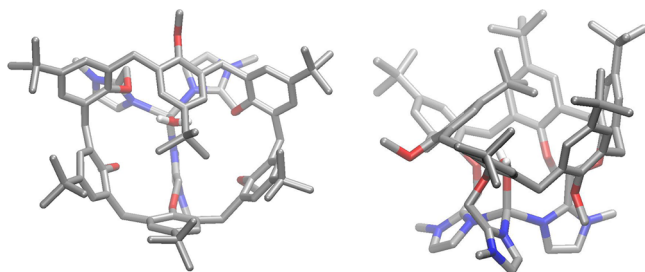

Figure 4. Top view (left) and side view (right) of CX_{2fs}. Most hydrogens are omitted for clarity.

Top and side views of CX_{3fs} are shown in Figure 3. The three phenyl units attached to OMe groups pitch in toward the C_3 axis, forming a funnel shape over the Zn−aqua center. The OMe groups point outside into solvent away from the catalyst core. The other three alternating phenyl units (attached to N-Me imidazoles) extend out from the C_3 axis, which minimizes steric hindrance between adjacent t-butyl groups. The aqua ligand forms a weak hydrogen bond between one of its

hydrogens and a calixarene arm oxygen. The average interatomic distance between the two oxygens involved was found to be 3.09 ± 0.13 Å, as calculated from a 5.5 ns unrestrained simulation of CX_{3fs}. This H bond pulls the aqua ligand away from its T_d symmetry above Zn, leaving Zn partially exposed, and is responsible for the distortion in 3fs symmetry.

We note that the complexes as studied (R = Me in Figure 2) are expected to have very low water solubility. The three OR groups extend into the solvent, suggesting that solubilizing groups (e.g., PEG chains or sulfonates) could be attached at this location to impart solubility without significantly perturbing the overall cavity geometry. It is possible that R containing electron-donating or -withdrawing substituents could change electronic properties at Zn^{2+}. Particularly, strongly electron-donating groups may be expected to reduce the Lewis acidity of Zn^{2+}, causing a more weakly associating aqua ligand and higher pK_a. In this work, we focus on the R = Me complex only, for reasons of computational efficiency.

Top and side views for CX_{2fs} are shown in Figure 4. The main structural difference is that one phenyl ring is collapsed over the Zn−aqua center, removing the cavity. This conformation may be stabilized by an OH/π noncovalent interaction; similar interactions involving Zn-bound adducts with calixarene aromatic walls have been reported experimentally.[26]

The PMF connecting CX_{3fs} and CX_{2fs} was calculated with R taken as the distance between aqua oxygen and the C4 carbon (attached to the t-butyl group) of one phenyl ring. The definition of R is shown graphically in the inset of Figure 5.
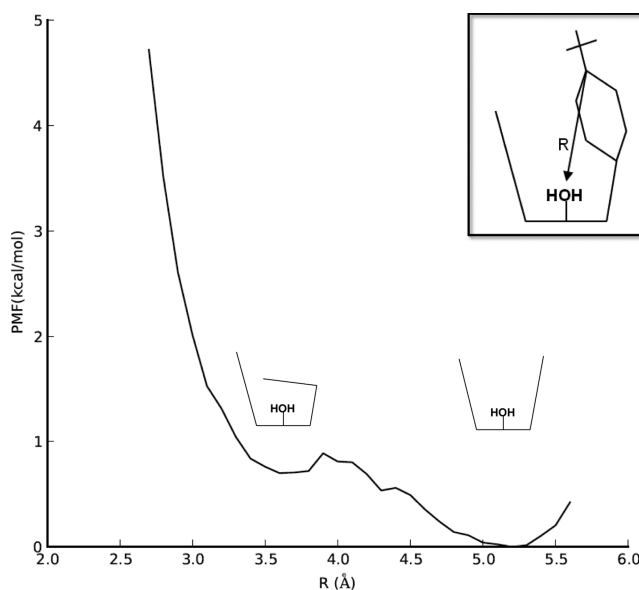

Figure 5. PMF connecting CX_{3fs} and CX_{2fs}. R equals the distance between the aqua ligand oxygen atom and C4 carbon atom of one phenyl ring (shown in the inset).

This choice was found to provide a smooth transition between CX_{3fs} and CX_{2fs}. Because this PMF involved large changes in calixarene conformation, separate partial charges were calculated at each value of R (from a random configuration within the window) before starting production MD runs. The PMF is shown in Figure 5. CX_{3fs} is calculated to be lower in energy by only 0.7 kcal/mol. The M06-2X/6-31G(d) energy ordering at

the gas-phase equilibrium geometries is 4.4 kcal/mol, with CX_{3fs} being lower in energy. The gas-phase energy ordering agrees with the calculated free-energy ordering. In solution, the calculated free-energy barrier is 0.9 kcal/mol from the CX_{3fs} minimum. While the quantitative values (<1 kcal/mol) are likely within the total error bars of the calculation, the results suggest that the empty calixarene cavity is extremely floppy in solution.

3.2. Encapsulation of Water and Comparison with Crystal Structure. Because an encapsulated substituent prevents the cavity from closing, only the 3fs geometry is accessible. The structure with an encapsulated water molecule, CX_{3fs}-H_2O, is shown in Figure 6. This geometry is very similar
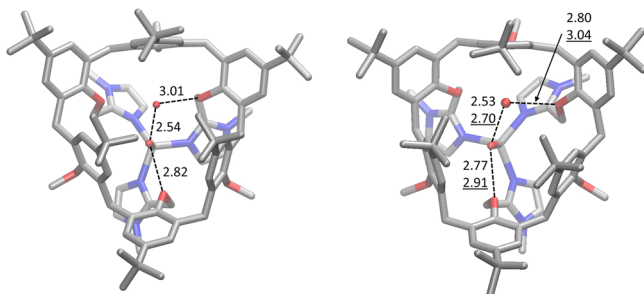

Figure 6. Geometries and relevant O−O hydrogen-bond distances in CX_{3fs}-H_2O. Left: X-ray crystal structure from ref 38. Some atoms are omitted for clarity. Right: M06-2X/6-31G(d) equilibrium geometry with DFT distances (normal text) and averaged MD distances (underline). Standard deviations for averaged MD distances are included in the text.

to the crystal structure reported by Reinaud.[38] Figure 6 shows the experimental crystal structure (left) and the DFT equilibrium geometry (right). The O−O hydrogen bond distances are labeled on both structures. The encapsulated ("buried") water sees the same hydrogen bonding environment in all three structures. The aqua ligand donates both hydrogens, one to a calixarene arm oxygen and the other to the buried water. The crystal structure shows the H bond between the aqua ligand and buried water to be extremely strong, due to the short, 2.54 Å distance. DFT is able to capture the strong nature of this H bond, with an O−O distance of 2.53 Å. MD recovers this H bond but not its very strong character (average O−O distance from an unconstrained simulation is 2.70 ± 0.11 Å). A hydrogen bond also exists between the buried water hydrogen and a (second) calixarene arm oxygen. This O−O distance is 3.01 Å in the crystal structure, 2.80 Å in the DFT structure, and 3.04 ± 0.29 Å in MD. In this case, DFT underestimates the distance relative to the crystal structure. All three structures reveal the same distorted T_d symmetry around Zn^{2+} as well as the same hydrogen bonds inside the cavity. Importantly, the agreement between theory and experiment suggests that MD and M06-2X/6-31G(d) computational methods may be used to accurately model noncovalent interactions within this complex.

The PMF for a water molecule traveling reversibly between the cavity and solvent was calculated, giving the free-energy difference between CX_{3fs} and CX_{3fs}-H_2O. R was taken as the distance between the water and aqua ligand oxygen atoms. The calculated PMF is shown in Figure 7. Implicit in the umbrella-sampling calculations is that within the time scale of the simulation, the system does not convert back to CX_{3fs}-H_2O for long R. As a result, the MD samples only configurations containing an empty cavity. The two states are close in free-
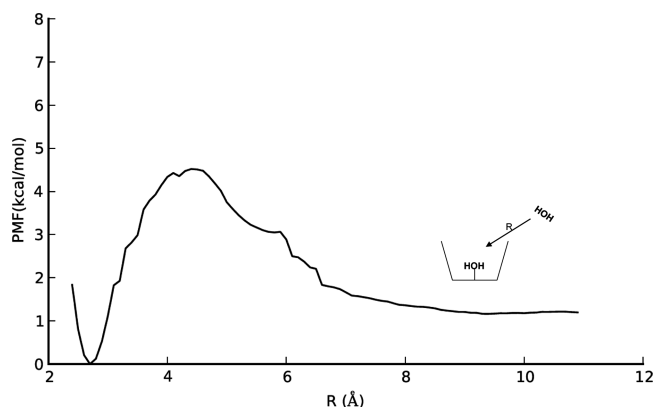

Figure 7. PMF connecting CX_{3fs} and CX_{3fs}−H_2O. R equals the distance between the aqua ligand oxygen atom and the water oxygen atom.

energy; CX_{3fs}−H_2O is calculated to be the global minimum by 1.2 kcal/mol. The small stabilization energy of water by the cavity suggests that it should be very labile to displace. The small value of the energy difference (1.2 kcal/mol) is likely too small to conclusively assign the ordering of the states, but it suggests that a buried water is energetically accessible in aqueous solution as well as under the crystallization conditions in ref 26. The barrier height for water to exit the cavity is also fairly small (4.5 kcal/mol), suggesting that water-molecule exchange between cavity and solvent is relatively facile. This may have important implications for step 3 of the catalytic cycle because deprotonation of the aqua ligand is likely to be water-mediated, in analogy with the enzyme. Visual analysis of trajectories at the barrier (R = 4.4 Å) showed that the water passes inside the volume enclosed by the *t*-butyl groups. A representative snapshot of the system at the barrier is shown in Figure 8. The water retains one hydrogen bond with a molecule
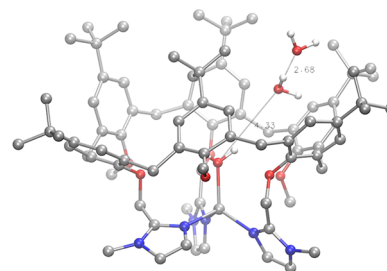

Figure 8. Representative MD snapshot from the barrier (R = 4.4 Å) in Figure 7. A hydrogen bond is maintained with a solvent molecule (O−O distance of 2.68 Å in the figure).

from the solvent; this solvent molecule can also penetrate into the hydrophobic volume. The hydrogen bond is expected to stabilize the transition state, because full desolvation of the entering water is not required. At smaller R, H bonds are established with both the calixarene arm oxygen and the aqua ligand.

As shown in Figure 7, there is a small barrier of 3.3 kcal/mol for a solvent molecule to enter the *t*-butyl groups of the *empty* cavity. When the cavity contains one encapsulated water (the global free-energy minimum), the barrier for this solvent molecule to access the *t*-butyl groups is expected to be less than 3.3 kcal/mol, because of additional hydrogen bonds that can be formed with the encapsulated water. These factors suggest that

the formation of connected H-bond networks between the cavity interior and external solvent, which should facilitate the proton-transfer step (step 3), does not encounter high free-energy barriers.

The discussion of step 3 in this calixarene complex and CA is qualitatively different from first-coordination sphere catalysts such as cyclen. In cyclen, the Zn-aqua group is exposed to solvent, so that the barriers for deprotonation and proton removal are replaced by a single pK_a corresponding to a fast equilibrium.[16,24]

In principle, the cavity may also be hydrated by two or more waters. This would be expected to help step 3 by establishing a connected water network between the aqua ligand and solvent. Connected water networks can allow faster proton removal, because they do not rely on significant motion of heavy atoms. We ran equilibrium simulations starting from several configurations with two encapsulated waters; these trajectories always ejected one water within the span of 100−200 ps. Several 11 ns trajectories were carried out with two water molecules inside the cavity, either with one or both waters restrained. Removal of the restraints after 11 ns (allowing significant time for relaxation of the solvent structure) in every case led to ejection of one of the water molecules within 100−200 ps. This suggests that there is no free-energy minimum for the calixarene cavity encapsulating two water molecules.

3.3. Encapsulation of CO_2 and HCO_3^-. Rapid sequestration of CO_2 out of solution into the catalytic active site can increase the overall catalytic rate. CO_2 is hydrophobic and might be expected to efficiently pass through the t-butyl groups relative to the polar H_2O molecule. Once inside the cavity, CO_2 is near the charged Zn-aqua core, which is not screened by a first solvation shell (unlike catalysts lacking a second-coordination sphere). The calculated PMF connecting CX_{3fs} and an encapsulated CO_2 molecule (labeled CX_{3fs}-CO_2) is shown in Figure 10. R was taken to be the distance between the
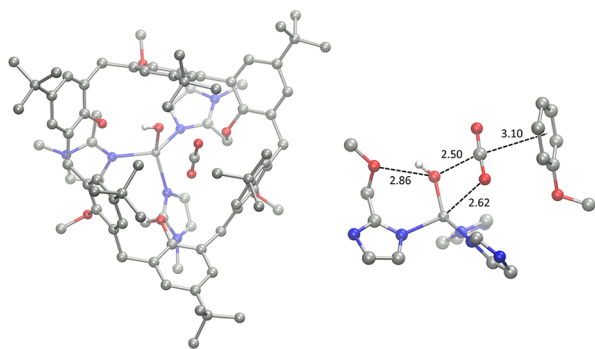

Figure 9. Top view (left) and side view (right) of the Zn-bound hydroxide complex with encapsulated CO_2. In the side view, most calixarene atoms have been removed except for the closest phenyl ring to CO_2.

aqua oxygen and the CO_2 carbon. The PMF shows a weak encounter complex forming as CO_2 approaches the calixarene from solution. Visual analysis of the trajectories around $R = 7.5$ showed that CO_2 is stabilized around the t-butyl groups. The encounter complex provides about 1.0 kcal/mol stabilization. From this minimum, the barrier for CO_2 entering into the volume enclosed by the t-butyl groups is 1.3 kcal/mol. This small barrier suggests that CO_2 entry into the empty cavity is highly favored. The difference in stabilization energies for CO_2 vs H_2O (2.7 kcal/mol vs 1.0 kcal/mol, respectively) suggests
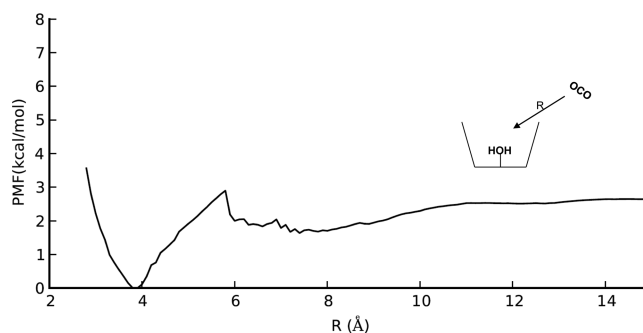

Figure 10. PMF connecting CX_{3fs} and CX_{3fs}−CO_2. R equals the distance between the aqua ligand oxygen atom and the CO_2 carbon atom.

that CO_2 will preferentially displace water from the cavity, although the kinetic barrier for this displacement process is not studied. On the basis of the attractive free-energy well for $R = 6−10$ Å in Figure 10, it seems likely that the calixarene can pull one or several CO_2 molecules into the vicinity of the cavity entrance, therefore keeping a high local CO_2 concentration to facilitate the overall rate of hydration. We note that the PMF contains the protonated aqua ligand, Zn−H_2O. This allows for uniform comparison of the different PMFs obtained in this work. However, the reactive complex involves CO_2 reacting with the deprotonated complex, Zn−OH^-. We expect that the initial entry of CO_2 through the t-butyl groups is relatively unaffected by the protonation state of the aqua ligand. In the next section, we analyze the reactive complex of CO_2 encapsulated with the deprotonated aqua ligand.

Figure 11 shows the corresponding PMF for HCO_3^- between the cavity and solvent. The steep slope shows that
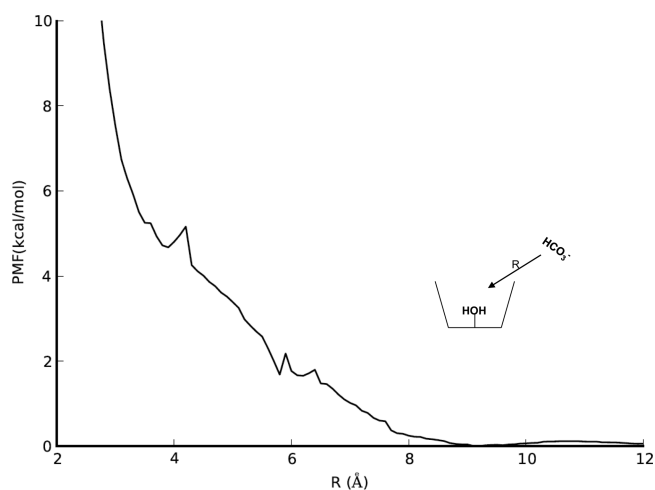

Figure 11. PMF connecting CX_{3fs} and CX_{3fs}-HCO_3^-. R equals the distance between the aqua ligand oxygen atom and the HCO_3^- carbon atom.

bicarbonate is strongly repulsed in all (nonbonded) regions of the PMF. Specifically, the nonbonded regime of the PMF exists for $R > 4$ Å, where 4 Å approximately corresponds to the onset of the van der Waals repulsive region. For decreasing R, the PMF rapidly diverges according to the repulsive vdW terms in the force field, which cannot account for quantum-mechanical interactions at shorter interatomic distances. Therefore, the PMF is only valid for large R values. The repulsive character of

the PMF for $R = 4-10$ Å in Figure 11 suggests that rapid expulsion of HCO_3^- will occur following the substitution reaction (step 2) in the catalytic cycle. Moreover, an external HCO_3^- concentration (e.g., from buffer) faces the same repulsive potential upon entering the cavity. This fact is promising because it can potentially be used to block reversibility of the CO_2 hydration reaction. Reversibility is a key feature in CA and is pH-dependent. At low pH, CA helps to deacidify the medium by catalyzing CO_2 formation (which is sparingly soluble and can be exhaled). However, blocking reversibility of CO_2 hydration is needed in industrial biomimetic catalysts. The calixarene cavity can achieve this by having fairly rigid, hydrophobic walls, which repel the charged bicarbonate ion as it tries to penetrate from solution into the active site. The qualitative shape of this PMF should be similar for other charged and highly polar species, allowing calixarene cavities to possibly exclude a variety of anionic inhibitors which form irreversible bonds to Zn^{2+}.

3.4. DFT Geometry Optimizations of Encapsulated CO_2 in the Hydroxide-Bound Species.

Step 1 in the catalytic cycle involves the nucleophilic addition of CO_2 to Zn-bound hydroxide. The PMF in Figure 10 shows that CO_2 has facile entrance into the (protonated) complex from outside solution. Geometry optimization of the deprotonated, *hydroxide* complex with encapsulated CO_2 was performed to analyze how the calixarene second-coordination sphere affects positioning of reactants inside the cavity. Particularly, the calixarene arm oxygens are located at similar distances from the aqua ligand as in CA, and the phenyl groups can potentially play the role of hydrophobic residues in the CA active site.

The optimized geometry is shown in Figure 9. The CO_2 molecule is located against a phenyl ring; the distance between the six aromatic carbons' center-of-mass and the CO_2 carbon is 3.10 Å. Notably, a CO_2 oxygen forms a strong, 2.62 Å interaction with Zn; this interaction becomes a Zn−O bond of the bicarbonate product. The interaction of this oxygen with Zn displaces OH^- from its tetrahedral position at Zn; this displacement is also stabilized by a hydrogen bond between the hydroxide and the calixarene arm oxygen distal to the CO_2. The hydroxide lone pairs are thus pointed toward the CO_2 carbon, in analogy with the enzyme. The $O(OH^-)$ to $C(CO_2)$ distance is 2.50 Å. The equilibrium structure in Figure 9 suggests that the calixarene arm oxygen and a phenyl unit work in tandem to preorganize the reactants inside the cavity for efficient nucleophilic addition. The calixarene arm oxygen can be considered a structural analog of Thr199, while the distal phenyl ring (Figure 9, right) can be considered an analog of two hydrophobic residues, Trp209 and Val143.

3.5. Conclusions.

The free-energy surface of a tris-(imidazolyl) calix[6]arene Zn aqua complex was characterized. The global free-energy minimum in water was found to contain one encapsulated water molecule, which is stabilized by a conserved network of three hydrogen bonds (Figure 6). Comparison of MD and DFT-optimized structures of the calculated global minimum are in close agreement with the experimentally reported crystal structure.[38] Conformations containing two encapsulated water molecules were not stable, as shown by unrestrained MD simulations which ejected the excess water molecule on a fast time scale (<200 ps).

Umbrella-sampling free-energy calculations showed that CO_2 has facile entrance into the hydrophobic cavity, proceeding through a small barrier of 1.3 kcal/mol from an encounter complex which stabilizes CO_2 molecules in the vicinity of the *t*-

butyl groups. In contrast, the bicarbonate ion experiences strong repulsive forces in all (nonbonded) regions of the calixarene pocket (Figure 11). This suggests fast product release following displacement of bicarbonate by a water molecule at the Zn site and may be an attractive approach to preventing reversibility of the catalytic cycle by lowering the effective HCO_3^- concentration around Zn.

M06-2X/6-31G(d) optimization of the reactive hydroxide complex with encapsulated CO_2 found that the cavity directs the reactants, through multiple noncovalent interactions, into a geometry well-suited for their nucleophilic addition. These interactions were shown to provide a large structural effect pulling Zn-bound OH^- away from T_d geometry and directing its lone pairs toward the CO_2 carbon.

On the basis of the current results, we suggest that the incorporation of second-coordination spheres into current designs should consider these three factors. First, the second-coordination sphere should provide a hydrogen-bond acceptor within close distance (< 3 Å) of the Zn-bound water. Second, the entrance of the pocket should be hydrophobic to facilitate CO_2 entry and HCO_3^- release. Third, the hydrophobic groups must allow solvent molecules to form H bonds with encapsulated molecules with low free-energy barriers, in order to facilitate proton transfer in analogy with CA. These factors have the potential to improve upon current first-coordination sphere designs such as aza-macrocyclic ligands, as well as providing a more realistic mimic of the CA enzyme.

A detailed knowledge of the multitude of noncovalent interactions of small-molecule substituents inside supramolecular cavities is important for the design of high-activity biomimetics for industry and biotechnology. Understanding these processes computationally in model compounds, which can be synthetically functionalized in a controlled manner, can allow for efficient testing of theoretical predictions. Finally, these calculations can shed light on the equivalent processes in the parent enzymes.

■ ASSOCIATED CONTENT

Ⓢ Supporting Information

Figure comparing simulation time for HCO_3^- PMF; figure comparing PMFs generated with eq 2 with WHAM analysis; Cartesian coordinates for M06-2X/6-31G(d) equilibrium geometries of $CX_{3fs}-H_2O$ and the hydroxide−CO_2 complex. This information is available free of charge via the Internet at http://pubs.acs.org/.

■ AUTHOR INFORMATION

Corresponding Author

*E-mail: aines1@llnl.gov, lightstone1@llnl.gov.

Notes

The authors declare no competing financial interest.

■ REFERENCES

(1) Khalifah, R. G. *J. Biol. Chem.* **1971**, *246*, 2561−2573.

(2) Lindskog, S. *Pharmacol. Ther.* **1997**, *74*, 1−20.

(3) Zhang, X.; Hubbard, C. D.; van Eldik, R. *J. Phys. Chem.* **1996**, *100*, 9161−9171.

(4) Campbell, I. D.; Lindskog, S.; White, A. I. *J. Mol. Biol.* **1974**, *90*, 469−489.

(5) Lindskog, S.; Silverman, D. N. *EXS* **2000**, *90*, 175−195.

(6) Silverman, D. N. *Acc. Chem. Res.* **1988**, *21*, 30−36.

(7) Maupin, C. M.; McKenna, R.; Silverman, D. N.; Voth, G. *J. Am. Chem. Soc.* **2009**, *131*, 7598−7608.

(8) Silverman, D. N.; McKenna, R. *Acc. Chem. Res.* **2007**, *40*, 669−675.

(9) Tu, C.; Silverman, D. N. *Biochemistry* **1989**, *28*, 7913−7918.

(10) Liang, Z.; Xue, Y.; Behravan, G.; Jonsson, B.; Lindskog, S. *Eur. J. Biochem.* **1993**, *211*, 821−827.

(11) Miscione, G. P.; Stenta, M.; Spinelli, D.; Anders, E.; Bottoni, A. *Theor. Chem. Acc.* **2007**, *118*, 193−201.

(12) Merz, K. M.; Banci, L. *J. Am. Chem. Soc.* **1997**, *119*, 863−871.

(13) Cui, Q.; Karplus, M. *J. Phys. Chem. A* **2003**, *107*, 1071−1078.

(14) Mauksch, M.; Brauer, M.; Weston, J.; Anders, E. *ChemBioChem* **2001**, *2*, 190−198.

(15) Zhang, X.; van Eldik, R.; Koike, T.; Kimura, E. *Inorg. Chem.* **1993**, *32*, 5749−5755.

(16) Zhang, X.; van Eldik, R. *Inorg. Chem.* **1995**, *34*, 5606−5614.

(17) Nakata, K.; Shimomura, N.; Shiina, N.; Izumi, M.; Ichikawa, K.; Shiro, M. *J. Inorg. Biochem.* **2002**, *89*, 255−266.

(18) Brown, R. S.; Salmon, D.; Curtis, N. J.; Kusuma, S. *J. Am. Chem. Soc.* **1982**, *104*, 3188−3194.

(19) Kimblin, C.; Murphy, V. J.; Hascall, T.; Bridgewater, B. M.; Bonanno, J. B.; Parkin, G. *Inorg. Chem.* **2000**, *39*, 967−974.

(20) Huang, D.; Makhlynets, O. V.; Tan, L. L.; Lee, S. C.; Rybak-Akimova, E. V.; Holm, R. H. *Proc. Natl. Acad. Sci. U. S. A.* **2011**, *108*, 1222−1227.

(21) Kato, M.; Ito, T. *Inorg. Chem.* **1985**, *24*, 509−514.

(22) Shengli, G.; Shengming, L.; Yuanqi, Y.; Kaibei, Y. *J. Coord. Chem.* **2011**, *46*, 145−157.

(23) Looney, A.; Saleh, A.; Zhang, Y.; Parkin, G. *Inorg. Chem.* **1994**, *33*, 1158−1164.

(24) Koziol, L.; Valdez, C. A.; Baker, S. E.; Lau, E. Y.; Floyd-III, W. C.; Wong, S. E.; Satcher, J. H., Jr.; Lightstone, F. C.; Aines, R. D. *Inorg. Chem.* **2012**, *51*, 6803−6812.

(25) Davy, R. *Energ. Proc.* **2009**, *1*, 885−892.

(26) Seneque, O.; Giorgi, M.; Reinaud, O. *J. Chem. Soc., Chem. Commun.* **2001**, 984−985.

(27) Case, D. A.; Darden, T. A.; Cheatham, T. E., III; Simmerling, C. L.; Wang, J.; Duke, R. E.; Luo, R.; Crowley, M.; Walker, R. C.; Zhang, W.; Merz, K. M.; Wang, B.; Hayik, S.; Roitberg, A.; Seabra, G.; Kolossvary, I.; Wong, K. F.; Paesani, F.; Vanicek, J.; Wu, X.; Brozell, S. R.; Steinbrecher, T.; Gohlke, H.; Yang, L.; Tan, C.; Mongan, J.; Hornak, V.; Cui, G.; Mathews, D. H.; Seetin, M. G.; Sagui, C.; Babin, V.; Kollman, P. A. *AMBER 10*, University of California: San Francisco, 2008.

(28) *Maestro*, version 9.2; Schrödinger, LLC: New York, 2011.

(29) Wang, J.; Wolf, R. M.; Caldwell, J. W.; Kollman, P. A. *J. Comput. Chem.* **2004**, *25*, 1157−1174.

(30) Lin, F.; Wang, R. *J. Chem. Theory Comput.* **2010**, *6*, 1852−1870.

(31) Valiev, M.; Bylaska, E. J.; Govina, N.; Kowalski, K.; Straatsma, T. P.; Dam, H. J. J. V.; Wang, D.; Nieplocha, J.; Apra, E.; Windus, T. L.; de Jong, W. A. *Comput. Phys. Commun.* **2010**, *181*, 1477−1489.

(32) Trzesniak, D.; Kunz, A. E.; van Gunsteren, W. F. *ChemPhysChem* **2007**, *8*, 162−169.

(33) Karim, O. A.; McCammon, J. A. *J. Am. Chem. Soc.* **1986**, *108*, 1762−1766.

(34) Kim, H.; Goddard, W. A., III; Jang, S. S.; Dichtel, W. R.; Heath, J. R.; Stoddart, J. F. *J. Phys. Chem. A* **2009**, *113*, 2136−2143.

(35) WHAM: the weighted histogram analysis method, version 2.0.6. http://membrane.urmc.rochester.edu/content/wham (accessed Jan. 4, 2013).

(36) Zhao, Y.; Truhlar, D. G. *Acc. Chem. Res.* **2008**, *41*, 157−167.

(37) Amin, E. A.; Truhlar, D. G. *J. Chem. Theory Comput.* **2008**, *4*, 75−85.

(38) Seneque, O.; Rager, M. N.; Giorgi, M.; Reinaud, O. *J. Am. Chem. Soc.* **2001**, *123*, 8442−8443.